Applied Catalysis B: Environmental 142–143 (2013) 205–213

Contents lists available at SciVerse ScienceDirect

Applied Catalysis B: Environmental

journal homepage: www.elsevier.com/locate/apcatb

In situ FT-IR study of the adsorption and photocatalytic oxidation of ethanol over sulfated and metallized TiO_2

J.J. Murcia[a,*], M.C. Hidalgo[a], J.A. Navío[a], J. Araña[b], J.M. Doña-Rodríguez[b]

[a] Instituto de Ciencia de Materiales de Sevilla (ICMS), Consejo Superior de Investigaciones Científicas CSIC – Universidad de Sevilla, Américo Vespucio 49, 41092 Sevilla, Spain

[b] CIDIA (Departamento de Química), Universidad de las Palmas de Gran Canaria, Edificio del Parque Científico Tecnológico, Campus Universitario de Tafira, 35017 Las Palmas de Gran Canaria, Spain

ARTICLE INFO

Article history:
Received 18 March 2013
Received in revised form 8 May 2013
Accepted 12 May 2013
Available online 21 May 2013

Keywords:
Sulfated TiO_2 photocatalysts
Pt-TiO_2
Au-TiO_2
Ethanol photo-oxidation
FT-IR

ABSTRACT

TiO_2 Degussa P25, TiO_2 prepared by sol–gel submitted to sulfation pre-treatment and some metallized catalysts obtained by photodeposition of Au or Pt over the sulfated TiO_2, were evaluated in the reaction of ethanol photo-oxidation. FT-IR spectroscopy was used to investigate the surface features of the photocatalysts, identifying adsorbed species and following the evolution of intermediate products in the ethanol photo-oxidation reaction. Nature of surface acidity in terms of Brönsted and Lewis centers was also studied.

Results showed that sulfation pre-treatment and metallization were important factors influencing the selectivity. Acetaldehyde was the main oxidation product on sulfated TiO_2; in the case of P25 also acetates production was observed. The photodeposition of metals had a detrimental effect on the selectivity to acetaldehyde; on metallized catalysts the formation of stable secondary intermediates was detected.

Based on these findings, a reaction pathway for the ethanol photo-oxidation over the different photocatalysts, via acetaldehyde or via acetate formation is proposed.

1. Introduction

Over decades, the reactions of ethanol on catalytic materials have been studied with great interest. It is well known that ethanol can be selectively oxidized by thermal catalysis to acetaldehyde, acetic acid or ethyl acetate; all of them can be used either as final products or as feedstock in synthetic routes of different industrial compounds. Likewise, the ethanol oxidation has been selected as a model reaction for assessing the tendency of different catalysts to drive this reaction towards acetaldehyde production (dehydrogenation) or to secondary pathways [1–4].

The partial oxidation of alcohols to carbonylic derivatives is a demanding chemical transformation for the production of fine and special chemicals. Normally, in these procedures stoichiometric amounts of oxoacids or halogenated compounds are used, which do not conform to the principles of green chemistry [4]. Thus, the search of new catalysts able to induce the oxidation of organic substrates through an environmentally friendly and cheap process represents a major target from the synthetic and industrial perspective.

In this context, the partial photocatalytic oxidation of organic compounds over TiO_2 has attracted considerable attention, since this is a promising alternative from the green chemistry point of view. The photocatalytic process involves the photoexcitation of semiconducting TiO_2, which promotes valence band electrons to the conduction band thus leaving an electron deficiency or holes in the valence band. The resulting electron–hole pairs can migrate toward the catalyst surface and initiate redox reactions that may oxidize adsorbed organic molecules. In this process, oxygen provides a sink for electrons, forming superoxide ions $O_2^{\bullet -}$ and its protonated form of hydroperoxide $HO_2^{\bullet}$. Holes can react with water molecules (or hydroxide anions) to form $OH^{\bullet}$ radicals, or can also be filled by the adsorbed organic donor [5,6]. Thus, surface hydroxyl groups play an important role in the photo-oxidation processes through their interactions with photogenerated holes.

The activity of a TiO_2 powder depends on its bulk and surface properties coming from the synthetic process used. The preparation method can also greatly affect the hydroxylation state of the TiO_2 and therefore can have an important influence in its photoactivity [6,7].

On the other hand, it is generally accepted that one major drawback of TiO_2 is the high recombination rate of the electron–hole pair photogenerated, which reduces its photoefficiency. In order to enhance the TiO_2 photocatalytic activity, many strategies have been developed. One of them has been the oxide modification through

* Corresponding author. Tel.: +34 954489550; fax: +34 954460665.
E-mail addresses: jjuliejoseane@hotmail.com, juliejmm@cartuja.csic.es (J.J. Murcia).

0926-3373/$ – see front matter.
http://dx.doi.org/10.1016/j.apcatb.2013.05.022

the sulfation of the TiO_2 surface. Several studies have reported that sulfation pre-treatment of TiO_2 results in the anatase phase stabilization up to 700 °C and in the creation of bulk oxygen vacancies due to a dehydroxylation process of the excess of adsorbed protons, giving rise to a highly defective material. A high amount of superficial oxygen vacancies and a small fraction of rutile phase were believed to be the reasons for the enhancement in the UV-photocatalytic activity of the TiO_2 through the improvement of charge separation and carriers lifetime [8–10]. Also, it has been reported that the TiO_2 treatment with sulfuric acid could increase its photoactivity in different photo-oxidation reactions, although the mechanism is not completely clear [11–13].

Other of the strategies widely studied for TiO_2 photoactivity improvement has been noble metal nanoparticles deposition [14,15]. Au and Pt deposits can act as receptors and transmitters of the electrons photogenerated in the illuminated TiO_2 thus reducing the recombination rate and therefore improving the photocatalytic activity of this oxide. The enhancement (or not) of the photocatalytic activity of TiO_2 by metal deposition seems to depend on different factors such as the substrate to be degraded, amount of deposited metal, metal particle size and metal chemical state, among others [16–18].

There have been some studies devoted to the selective oxidation of alcohols to carbonyl compounds catalyzed by photoexcited TiO_2 [18–22]; however, the influence of the sulfation pre-treatment and noble metal deposition on the alcohols photo-oxidation reaction mechanism has received less attention and still a lot remains to be investigated. The objective of this study was to conduct the selective gas phase ethanol photo-oxidation on sulfated TiO_2 surface, with and without the addition of noble metals (Au and Pt) investigating the reaction pathways on the different samples. A comparative FT-IR study of the surface structure of these samples was also attempted; the evolution of adsorbed species under irradiation was conducted in an in situ IR cell.

2. Experimental

2.1. Synthesis of the photocatalysts

2.1.1. Titanium dioxide

Lab prepared TiO_2 was synthesized by sol–gel process. Firstly, titanium tetraisopropoxide (TTIP Aldrich, 97%) used as precursor was mixed with isopropanol to form a solution 1.6 M. Then, distilled water was slowly added to this solution to get a final volume ratio isopropanol/water 1:1. The obtained precipitate was recovered by filtration and dried at 110 °C for 24 h.

Afterward, the dry powder was sulfated by immersion in a 1 M sulfuric acid solution under continuous stirring for 1 h. The resulting amorphous titania was then transformed into crystalline TiO_2 by calcination at 650 °C for 2 h. Hereon, the material thus obtained will be denoted as "lp-TiO_2".

Commercial TiO_2 Degussa P25 was used as received. For comparison purposes sulfated Degussa P25 was also prepared by using the same procedure described above for the lp-TiO_2.

2.1.2. Metallized photocatalysts

The metallized samples were prepared by photodeposition of gold or platinum on lp-TiO_2 following a method described elsewhere [17,18]. The nominal amount of metal deposited was 0.5% in weight in every case.

Gold photodeposition was performed by suspending the lp-TiO_2 powder in an aqueous solution of Gold (III) chloride trihydrate ($HAuCl_4$, Aldrich 99.9%) containing isopropanol, which acts as sacrificial donor. The suspension was then illuminated under N_2 atmosphere for 120 min using an Osram Ultra-Vitalux lamp (300 W) with a sun-like radiation spectrum and a main emission line in the UVA range at 365 nm. The intensity of the lamp was 0.15 W/m^2. After photodeposition, the powders were recovered by filtration and dried at 110 °C overnight.

In the case of platinum photodeposition, hexachloroplatinic acid (H_2PtCl_6, Aldrich 99.9%) was used as metal precursor and the intensity of the lamp was 60 W/m^2.

2.2. Characterization of the photocatalysts

BET surface area and porosity measurements were carried out by N_2 adsorption at −195.8 °C and 1 atm, using a Micromeritics ASAP 2010 instrument.

UV–vis spectra were measured on a Varian spectrometer model Cary 100 equipped with an integrating sphere and using $BaSO_4$ as reference. Band-gaps values were calculated from the corresponding Kubelka–Munk functions, $F(R\infty)$, which are proportional to the absorption of radiation, by plotting $(F(R\infty)\cdot h\nu)^{1/2}$ against $h\nu$ [23].

Chemical composition and total metal content of the samples was determined by X-ray fluorescence spectrometry (XRF) in a PanalyticalAxios sequential spectrophotometer. XRF measurements were performed onto pressed pellets (sample included in 10 wt.% of wax).

X-ray diffraction (XRD) patterns were obtained on a Siemens D-501 diffractometer with Ni filter and graphite monochromator using Cu Kα radiation. Crystallite sizes were calculated from the line broadening of the main XRD peaks by using the Scherrer equation. Peaks were fitted by using a Voigt function.

Transmission electron microscopy (TEM) was performed in a Philips CM200 instrument. The samples were dispersed in ethanol using an ultrasonicator and dropped on a carbon grid. Determination of the metal particle average diameter ($\bar{d}$) in the metallized samples was accomplished by counting particles in a high number of TEM images from different places of the samples. The following equation was used: $\bar{d}\ (\mathrm{nm}) = \sum di \times fi$; where di is the diameter of the ni counted particles and fi is the particle size distribution estimated by: $fi = ni/\sum ni$; where ni is the number of particles of diameter di [24].

X-ray photoelectron spectroscopy (XPS) study was carried out on a Leybold-Heraeus LHS-10 spectrometer, working with constant pass energy of 50 eV. The spectrometer main chamber, working at a pressure < 2×10^{-9} Torr, is equipped with an EA-200 MCD hemispherical electron analyzer with a dual X-ray source working with Al Kα ($h\nu$ = 1486.6 eV) at 120 W and 30 mA. C 1s signal (284.6 eV) was used as internal energy reference in all the experiments. Samples were outgassed in the prechamber of the instrument at 150 °C up to a pressure < 2×10^{-8} Torr to remove chemisorbed water.

Fourier transform infrared (FT-IR) study of the photocatalysts and the monitoring of the photoactivity tests were carried out using a Thermo Scientific-Nicolet iS10 spectrophotometer. Intervals of 4000–1000 cm^{-1}, a resolution of 2 cm^{-1} and a forward and reverse moving mirrors speed of 10 and 6.2 kHz, respectively were used.

2.3. Photocatalytic tests

The photocatalytic activity of the samples was tested in the ethanol photo-oxidation reaction. Firstly, photocatalysts were impregnated with (3:1, v/v) vapor ethanol–water mixtures at room temperature. After 30 min of impregnation, photocatalysts were placed between two CaF_2 windows in a proper cell for FT-IR analysis. Once the initial FT-IR spectrum was obtained, the cell was irradiated successively (1–40 min) and analyzed by FT-IR again. A 60 W UV-lamp (Solarium Philips HB 175) equipped with four, 15 W Philips CLEO fluorescent tubes with emission spectrum from 300 to 400 nm (maximum around 365 nm) was used as UV-light source.

3. Results

3.1. Photocatalysts characterization

Lp-TiO_2 and lp-TiO_2 metallized with Au and Pt were widely characterized. P25 and eventually sulfated P25 were also studied as references.

A summary of the characterization results is presented in Table 1. As it can be seen, all the materials present very similar surface area (S_{BET}) values, ranging between 50 and 60 m^2/g. Only P25 (S) sample shows a lower S_{BET} value of 28 m^2/g.

Estimated band gap energies were ca. 3.2 eV for all the samples, not being affected by metal deposition.

XRF results for Au-TiO_2 and Pt-TiO_2 showed that metal content for both samples was lower than the theoretical nominal content of 0.5% (see Table 1) indicating an incomplete reduction of the metal precursors on the TiO_2 surface. Also the XRF analysis revealed that a certain amount of adsorbed S species (from sulfate groups) remained on the solid after preparation, i.e. 0.66, 0.22, 0.16 and 0.12% for lp-TiO_2, P25 (S), Au-TiO_2 and Pt-TiO_2 respectively.

Fig. 1 shows the XRD patterns for all samples. As expected, in the diffractogram of TiO_2 P25, peaks corresponding to anatase and rutile were detected (anatase to rutile ratio 80:20). After the sulfation treatment of P25, the proportion of rutile increased; thus, for P25 (S) sample the composition of crystalline phases was 72:28 for anatase and rutile respectively. This partial rutilization may be contributing to the lower surface area exhibited by this sample.

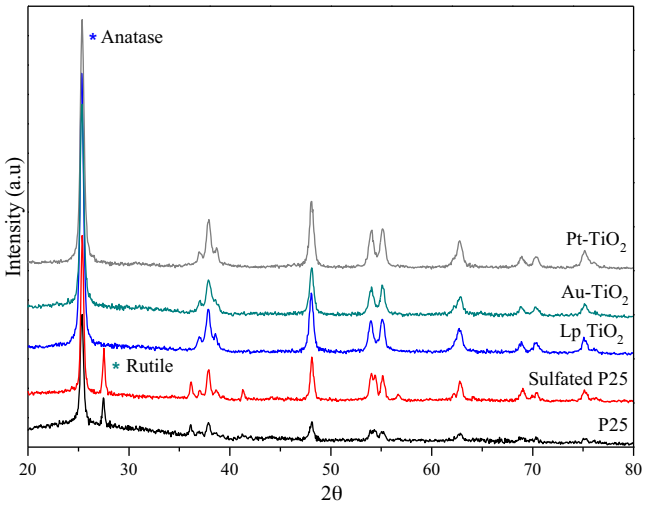

Fig. 1. XRD patterns for analyzed catalysts.

For all the rest of the samples, lp-TiO_2 and metallized lp-TiO_2, the only crystalline phase present was anatase. In the spectra of metallized samples, no diffraction peaks for Au or Pt were detected probably due to the low metal content and high dispersion of metal particles.

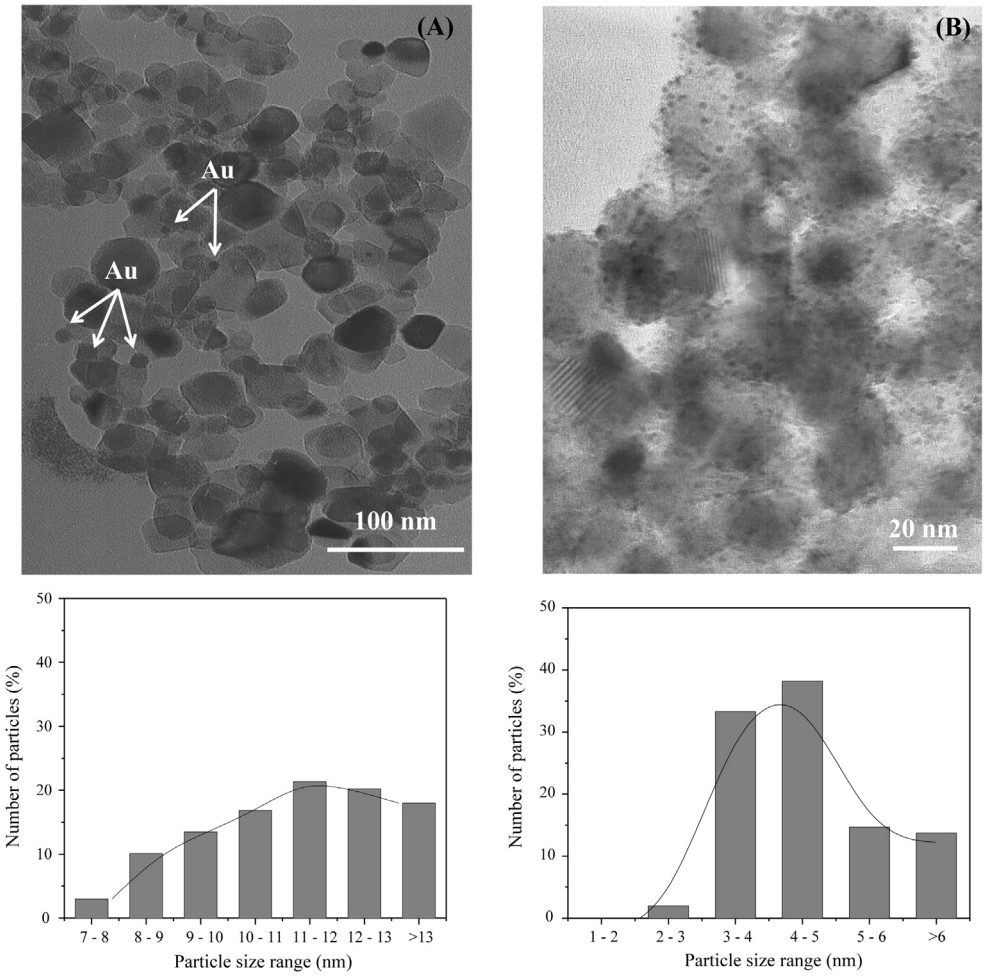

Fig. 2. TEM images and distribution of metal particle size for M-TiO_2 photocatalysts. (A) Au-TiO_2 and (B) Pt-TiO_2.

Table 1
Characterization results.

Catalyst	S_{BET} (m^2/g)	Band gap (eV)	Wt.% metal (XRF)	$D_{anatase}$ (nm)	$\bar{d}$ (nm)	Binding energy (eV)		O/Ti
						Ti $2p_{3/2}$	O 1s	
P25	51	3.23	–	22	–	458.5	529.8	1.87
P25 (S)	28	3.14	–	23	–	458.6	529.9	1.75
Lp-TiO_2	58	3.20	–	20	–	458.5	529.8	1.70
Au-TiO_2	60	3.20	0.37	19	11.2	458.5	529.8	1.88
Pt-TiO_2	49	3.17	0.30	20	4.5	458.4	529.6	1.91

The average anatase crystal size for all the samples estimated by the Scherrer equation was found to be in a range between 19 and 22 nm as shown in Table 1.

The morphology of the metallized samples was studied by TEM and selected micrographs are shown in Fig. 2. As it can be observed, in the Au-TiO_2 photocatalyst the gold particles are heterogeneously distributed over the TiO_2 surface (Fig. 2A). For this sample a wide range of particle sizes can be found, with particles ranging from 7 nm to diameters larger than 13 nm. On the contrary, in the Pt-TiO_2 photocatalyst (Fig. 2B) a narrow metal particle size distribution and high dispersion of platinum over the TiO_2 surface was observed. The estimated average particle size for this photocatalyst was 4 nm.

XPS measurements for all the samples were also performed; a summary of these results is reported in Table 1.

In the O 1s region, a peak located at binding energy of 529.6 ± 0.2 eV can be seen for all the samples, corresponding to O^{2-} in the TiO_2 network (Fig. 3(A)). In addition, broad shoulders at higher binding energies (530.3 eV) ascribed to oxygen in surface hydroxyl groups were also observed. On the other hand, the Ti 2p core level spectra were similar for all the studied samples with peaks of binding energies located at 458 ± 0.5 eV, ascribed to Ti^{4+} as the main component (Fig. 3(B)).

XPS results also showed that O/Ti atomic ratio in the lp-TiO_2 (no metallized) and P25 (S) was 1.70 and 1.75 respectively, implying that within the ca. 4 nm thickness analyzed by the XPS technique the ratio of these species is below the stoichiometric value and therefore a certain number of oxygen vacancies in the surface of the material should be expected. After the photodeposition of either Au or Pt, O/Ti ratio increased to values around 1.88 and 1.91 respectively, suggesting that oxygen vacancies were partially annihilated during the photodeposition process.

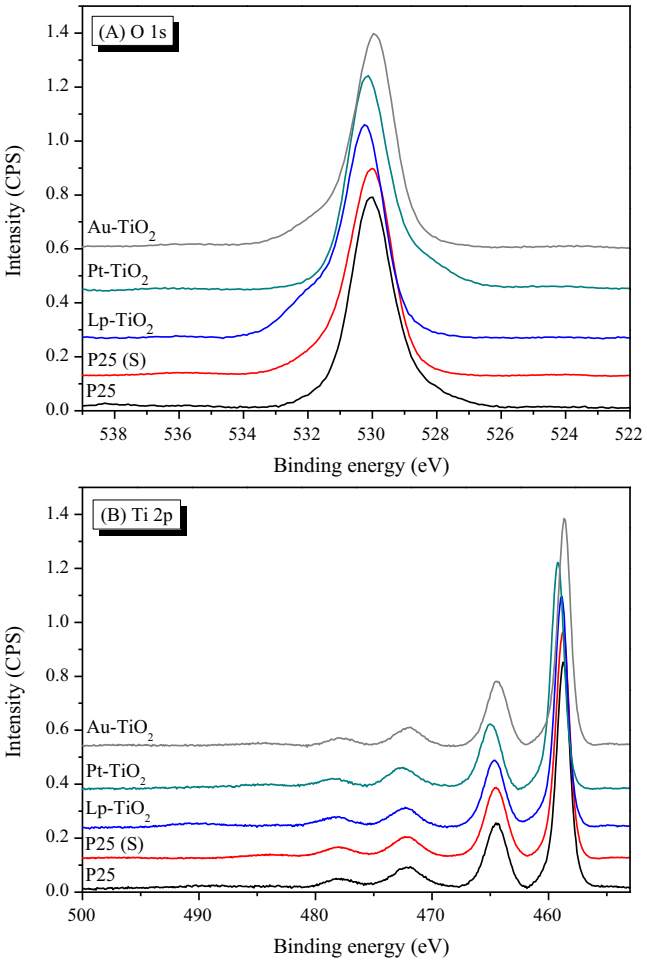

Fig. 3. XPS core level spectra of O 1s and Ti 2p for analyzed photocatalysts.

3.2. FT-IR study

3.2.1. Hydroxyl groups

The characterization of the hydroxyl groups distribution in the samples was attempted by FT-IR and the obtained spectra in the range between 4000 and 2400 cm^{-1} are presented in Fig. 4. As it can be observed, a band at 3698 cm^{-1} corresponding to isolated hydroxyl groups (Ti-$OH_{(is)}$) was detected in all the samples. The relative intensity of this band in the lp-TiO_2 and metallized samples is higher than the one observed in the P25 spectra, suggesting that on the P25 surface there is a lower amount of Ti-$OH_{(is)}$.

The specific infrared absorptions in the IR region between 3500 and 3150 cm^{-1}, corresponding to hydroxyl groups H-bounded, can also be observed in Fig. 4. Two clear bands located at 3393 cm^{-1} and at 3214 cm^{-1} were detected. These absorptions have been assigned to terminal Ti-OH and adsorbed water Ti-OH_2 species respectively [25]. In the lp-TiO_2 spectrum, the relative intensity of the band ascribed to terminal Ti-OH is lower than the band assigned to the Ti-OH_2 species.

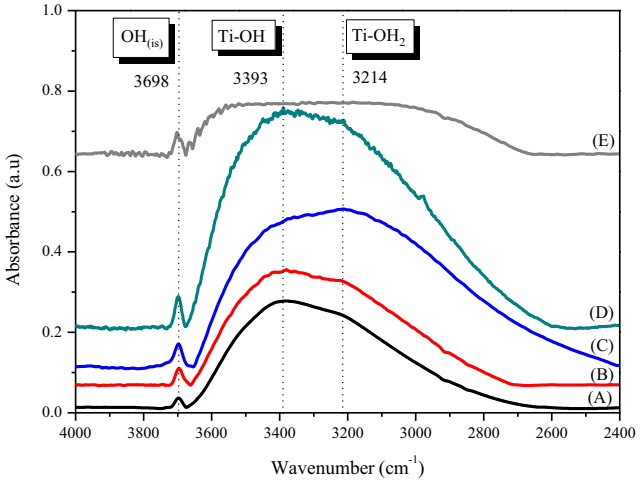

Fig. 4. FT-IR spectra in the region between 4000 and 2400 cm^{-1} (hydroxyl groups region). (A) P25; (B) sulfated P25; (C) lab prepared TiO_2; (D) Au-TiO_2 and (E) Pt-TiO_2.

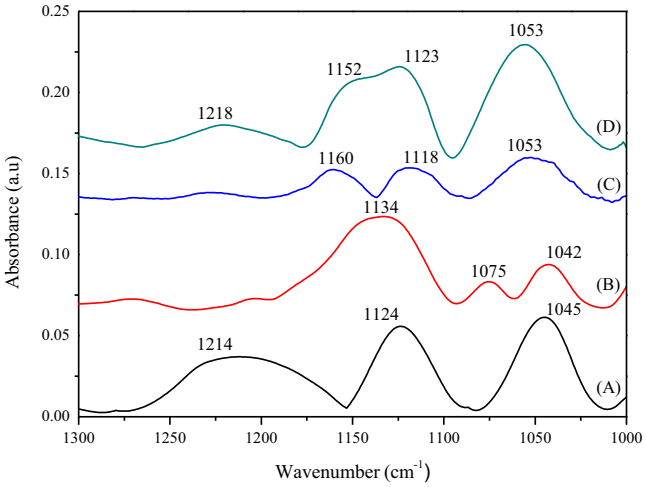

Fig. 5. FT-IR spectra for analyzed catalysts, surface sulfate groups. (A) Lab-prepared TiO_2; (B) sulfated P25; (C) Au-TiO_2 and (D) Pt-TiO_2.

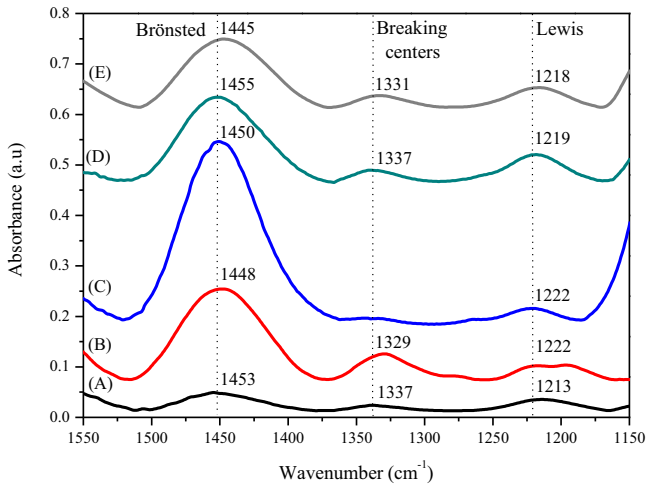

Fig. 6. Brönsted and Lewis sites in analyzed photocatalysts FT-IR study. (A) P25; (B) sulfated P25; (C) lab prepared TiO_2; (D) Au-TiO_2 and (E) Pt-TiO_2.

The spectra of the P25 pure and sulfated are very similar, only a slightly increase in the relative intensity of the band corresponding to Ti-$OH_{(is)}$ groups was detected for the later sample.

For metallized samples a different trend was observed. The Au-TiO_2 sample presents IR bands with the highest relative intensity compared to all the other analyzed materials, while in the case of the Pt-TiO_2 sample the corresponding IR bands have significant lower intensities, suggesting a lower degree of surface hydroxylation. This may be attributed to the high number of Pt particles all over the lp-TiO_2 surface as observed by TEM (Fig. 2A).

The FT-IR study agrees with the XPS outcomes, which have noticed the presence of surface hydroxyl groups in all the samples.

3.2.2. Sulfate groups

Fig. 5 shows the FT-IR spectra of all the analyzed photocatalysts in the range between 1300 and 1000 cm^{-1}. In this range it was possible to detect bands corresponding to sulfate species, suggesting that the calcination temperature used (650 °C) was not sufficient for the total elimination of sulfates from the TiO_2 [8], in agreement with XRF results. In the metallized samples, the sulfate species bands were also detected, indicating that these photocatalysts would preserve to a certain extent the sulfates from the starting sulfated TiO_2 precursor even after the photodeposition process.

In the literature, two infrared sulfate vibrations have been reported: the nondegenerate symmetric stretching ν_1 and the triply degenerate asymmetric stretching ν_3. As a free anion in solution, sulfate has tetrahedral symmetry; whereas, if sulfate forms a bidentate binuclear (bridging) surface complex, the symmetry is lowered to C_{2v}, and the ν_3 band splits into three bands between 1050 and 1250 cm^{-1}, while the ν_1 band is shifted to around 1000 cm^{-1} [26–29].

As shown in Fig. 5, in the lp-TiO_2 spectrum, two bands at 1045 and 1124 cm^{-1} and a wide band at 1214 cm^{-1} were detected. A comparison between this spectrum and others reported in the literature, leads us to confirm the presence of sulfate groups mono and bidentates on the surface of this catalyst [26–29].

On the other hand, as it was indicated in the experimental section, P25 was submitted to a sulfuric acid pre-treatment and the obtained spectrum is included in Fig. 5. For the sulfated P25 and the Au-TiO_2 photocatalyst three ν_3 bands at wavenumbers much higher than those for lp-TiO_2 were observed, indicating the presence of a bidentate mononuclear (chelating) surface complex [26]. In the case of Pt-TiO_2 photocatalyst the appearance of four bands could be interpreted as evidence of bidentate coordination; however, the fourth band could also reflect the formation of bisulfate or other protonated structures [27].

3.2.3. Brönsted and Lewis sites

Ammonia is frequently used as probe molecule for acidity assessment, because it can interact with both Brönsted acidic sites (by forming ammonium ions) and Lewis acidic sites (by forming acidic-basic adducts) [30,31].

In this work the Brönsted and the Lewis acid sites of the different photocatalysts were studied by FT-IR spectroscopy of adsorbed NH_3. The relationship between those sites and the interaction ethanol–photocatalyst was also analyzed.

Each sample was impregnated with vapor NH_3 dosed at room temperature for 30 min after which the infrared spectra were collected. FT-IR spectra obtained for the different TiO_2 powders analyzed in the range 1550–1150 cm^{-1} are presented in Fig. 6.

In the P25 spectrum three bands at 1453, 1337 and 1213 cm^{-1} were observed. These bands are assigned to Brönsted, breaking centers and Lewis sites respectively. A breaking center formation occurs in a surface on which coexist Brönsted and Lewis centers very close together, wherein the water molecule can be broken. It has been reported that NH_3 adsorption takes place on Lewis acid centers with the subsequent transformation to NH_2 species, it can be represented as follows [30,32,33] (M = adsorption centers):

$$NH_3 + M^{n+} + O^{2-} \rightarrow M^{(n-1)+} \ldots NH_2 + OH^-$$

In a similar way, for the breaking of the water molecule:

$$H_2O + M^{n+} + O^{2-} \rightarrow M^{(n-1)+} \ldots OH + OH^-$$

On the other hand, as it can be observed in Fig. 6, the relative intensity of all these bands in the P25 spectrum is lower than those for lp-TiO_2; and this is particularly evident for the signal at 1453 cm^{-1}.

Moreover, in lp-TiO_2, a shift of the band assigned to Lewis sites to higher wavenumber (1222 cm^{-1}) can be observed. This indicates that lp-TiO_2 has a higher acid character and a higher capacity to accept electrons than P25. The shifting of this band can be ascribed to the presence of sulfate groups on the lp-TiO_2 surface; indeed, as it can be observed in Fig. 6, lp-TiO_2 and sulfated P25 spectra are quite similar, corroborating this hypothesis.

In the case of metallized samples (Fig. 6) the bands corresponding to Lewis sites are also shifted to higher wavenumbers compared to those of P25. The IR band assigned to breaking centers at 1337 cm^{-1} observed in both pure and sulfated P25 does

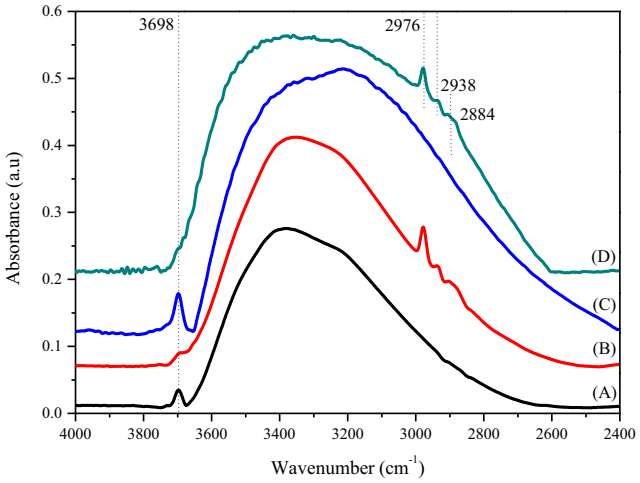

Fig. 7. FT-IR spectra for ethanol adsorption over analyzed catalysts, range between 4000 and 2400 cm^{-1}. (A) P25; (B) P25 + EtOH; (C) lab prepared TiO_2 and (D) lab prepared TiO_2 + EtOH.

practically not appear in the lp-TiO_2 spectrum. A slight growth of this band with the photodeposition of Au or Pt was also observed.

3.3. Photoreactivity results

The ethanol photo-oxidation reaction was carried out by impregnation of the photocatalysts with ethanol and further irradiation. A FT-IR analysis of the adsorbed species before and after the irradiation was performed.

3.3.1. Ethanol adsorption

In order to investigate the trend of ethanol adsorption onto the photocatalysts surface, some preliminary experiments were carried out without illumination. A comparison between the FT-IR spectra of P25 and lp-TiO_2 before and after the ethanol adsorption is presented in Fig. 7. The adsorption of ethanol on TiO_2 produces intense absorption bands in the IR spectrum, assigned to the vibrations of adsorbed ethoxy species [34]. Indeed in Fig. 7 (range of 4000–2400 cm^{-1}), it is possible to observe three clear ethanol bands at 2976 cm^{-1}, 2938 cm^{-1} and 2884 cm^{-1}, assigned to $\nu_{as}(CH_3)$, $\nu_{as}(CH_2)$ and $\nu_s(CH_3)$ vibrational modes respectively.

As it can be seen in Fig. 7, the relative intensity of the band at 3698 cm^{-1}, assigned to isolated OH, for P25 decreases notably after ethanol impregnation. In the case of lp-TiO_2 and metallized lp-TiO_2 (spectra not shown), this band completely disappears after ethanol adsorption. This indicates that the ethanol–catalyst interaction is taking place on the centers where the Ti-$OH_{(is)}$ groups were localized.

Fig. 8 shows the IR spectra of ethanol and the different ethanol impregnated samples in the range between 1600 and 1000 cm^{-1}. Five clear bands in the pure ethanol spectrum (symmetric and asymmetric deformations of CH_2 and CH_3 groups) can be identified. These bands are located at 1455 cm^{-1} ($\delta CH_{3as} + \delta CH_2$ vibrations); 1419 cm^{-1} (δOH); 1380 cm^{-1} (δCH_3) and 1089 and 1048 cm^{-1} (νC—C and νC—O vibrations respectively) [35,36].

As it can be seen in Fig. 8, in the spectrum corresponding to P25, the δOH vibration band located at 1419 cm^{-1} completely disappears after ethanol adsorption, probably due to the formation of an alcoholate (ethanolate). By contrast, in the spectra of lp-TiO_2 and in the metallized samples all bands of ethanol are present. This indicates that the ethanol–photocatalyst interaction is given here mainly by hydrogen bonding. However, on these photocatalysts the alcoholate formation cannot be ruled out.

3.3.2. Ethanol photo-oxidation

The evolution of the different adsorbed species onto the photocatalysts under irradiation was followed for 40 min. Acetaldehyde and acetates were identified by FT-IR as the main reaction products, the obtained spectra are represented in Fig. 9.

As it can be seen, under the same experimental conditions, the two titania powders analyzed (P25 and lp-TiO_2) exhibited a very different photocatalytic behavior. The absence of appreciable νC—C and νC—O stretching bands at 1089 and 1048 cm^{-1} after 11 min of irradiation for P25, suggests that ethanol was completely depleted after this time. On the contrary, the disappearance of the substrate was not complete even after 40 min of irradiation over the lp-TiO_2.

On the other hand, as it can be observed in Fig. 9, the irradiation of P25 containing ethanol, produces two bands at 1541 and 1440 cm^{-1}; these bands are ascribed to ν_{as}(COO)and ν_s(COO) vibration of adsorbed acetate (CH_3COO^-) respectively [34,35]. Carbonate species may also be detected in the region between 1450 and 1400 cm^{-1}. The acetate production could be understood considering that, as it has been already reported elsewhere [35], a high concentration of H-bounded hydroxyl groups favors the formation of ethoxides, which can be oxidized to acetates by means of the reaction with $OH^{\bullet}$ and $O_2^{\bullet -}$ radicals.

By contrast, it was found that lp-TiO_2 degrades ethanol to yield acetaldehyde (IR band at 1710 cm^{-1}) as the main reaction product and no acetate formation was detected with this photocatalyst. This behavior may result from the presence of sulfate groups on the lp-TiO_2 surface.

In order to understand the molecular phenomena involved in the ethanol oxidation on the P25 and to explain the differences in the photo-activity observed on the two TiO_2 powders studied, the ethanol photo-oxidation reaction was also carried out over a sulfated P25 sample. The obtained results led to conclude that the selectivity to acetaldehyde can be increased by sulfation pretreatment, since similarly to the lp-TiO_2; with the sulfated P25 (P25 (S)) the production of acetates was not detected. However in the spectrum of P25 (S) a new absorption IR band located at 1276 cm^{-1} was noticed (Fig. 9). This band can be assigned to adsorbed acetic acid.

In the metallized samples a quite different situation was observed. After irradiation of the Au-TiO_2 photocatalyst impregnated with ethanol, both acetate and acetaldehyde were detected. Over the Pt-TiO_2 photocatalyst the selectivity to acetaldehyde was lower than the obtained with Au-TiO_2. Besides, with the platinized sample a significant formation of some stable intermediate species during the irradiation was observed. The low H-bounded hydroxyl concentration observed in Pt-TiO_2 photocatalyst could favor the formation of the intermediate species, instead of the acetate production.

4. Discussion

In this study it was observed that the lp-TiO_2 (sulfated) photocatalysts presented a completely different photocatalytic behavior in the ethanol oxidation reaction than pure P25. After sulfation, P25 exhibited a similar activity to lp-TiO_2.

The differences observed in the mechanism of ethanol photo-oxidation over pure and sulfated samples may be due to the sulfate ions adsorbed on catalyst surface. The presence of sulfate species was verified by XRF, XPS and FT-IR analyzes.

It has been reported that the sulfate species adsorption on a given surface takes place mainly by substitution of M-OH_2^+ or M-OH groups, or by interaction with surface oxygen vacancies [37].

In this study, it was possible to identify the distribution of hydroxyl groups on the different materials by FT-IR (Fig. 3). In P25 and lp-TiO_2 catalysts two adsorption centers were observed; the

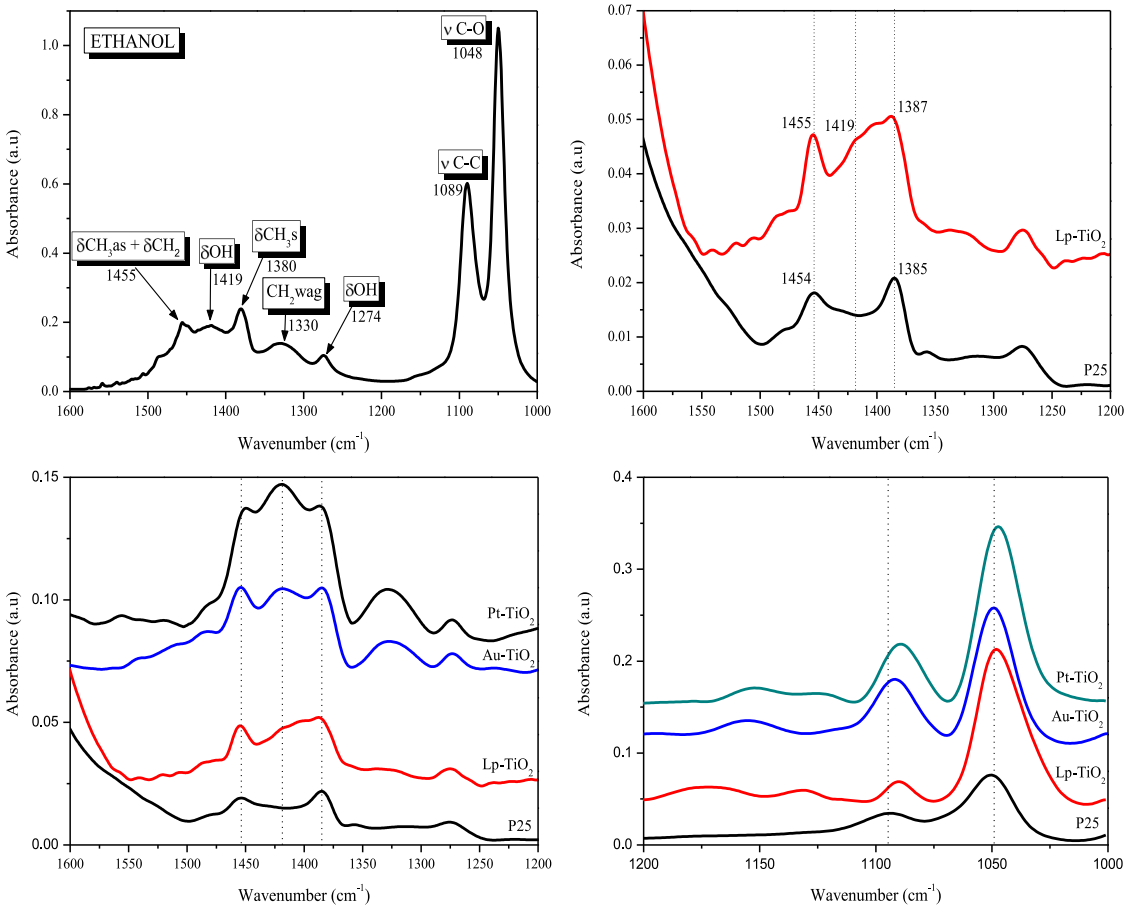

Fig. 8. FT-IR spectra between 1600 and 1000 cm^{-1} for ethanol adsorption on analyzed catalysts.

first one on the H-bounded hydroxyl groups region and the second one on isolated OH groups. As it was seen in Fig. 4, the lp-TiO_2 catalyst presented the highest relative proportion of adsorbed Ti-OH_2 species.

The FT-IR characterization analysis by NH_3 adsorption showed that on lp-TiO_2 no breaking centers are present; that is, there are no Lewis acid centers close to Brönsted acid sites where the breaking of water molecules can take place [32].

The absence of breaking centers on lp-TiO_2 would explain the highest relative proportion of Ti-OH_2 observed in this catalyst, as water breaking would be avoided.

On the other hand, it was also observed that lp-TiO_2 has a higher Lewis acid character than P25. However, it seems that Lewis centers are farther from the Brönsted acid centers in the lp-TiO_2; as a consequence of this the above mentioned breaking of water molecules is avoided on this catalyst. Taking into account these observations, the following schemes related to the distribution of the hydroxyl groups on each the catalysts surfaces are proposed (Schemes 1 and 2).

It was observed that the ethanol interaction with all analyzed catalysts, takes place on centers corresponding to isolated hydroxyl groups. These centers are related to oxygen vacancies or surface defects, which are the Lewis acid centers on catalyst surface with the highest acid character [38,39].

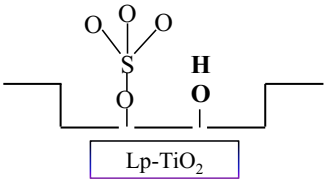

Scheme 2. Distribution of the hydroxyl groups on Lp-TiO_2 surface.

The alcohol interaction with lp-TiO_2 or P25 surfaces is very different. In the case of P25 the formation of an alcoholate was observed. On lp-TiO_2 this interaction is given mainly through hydrogen bonding. This trending could be related with the differences observed in the distribution of the acid centers of Lewis and Brönsted. Thereby, the closeness of both Lewis and Brönsted centers in the P25 surface favors the formation of alcoholate species (Scheme 3).

In the case of lp-TiO_2, the ethanol–catalyst interaction by hydrogen bonding could be due to an effect of the sulfate ions on the

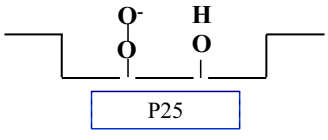

Scheme 1. Distribution of the hydroxyl groups on P25 surface.

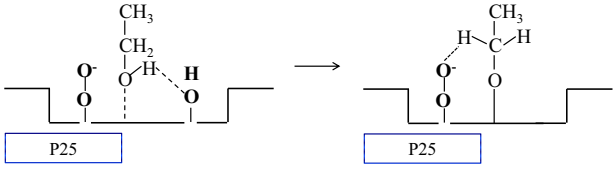

Scheme 3. Ethanol–P25 interaction via alcoholate formation.

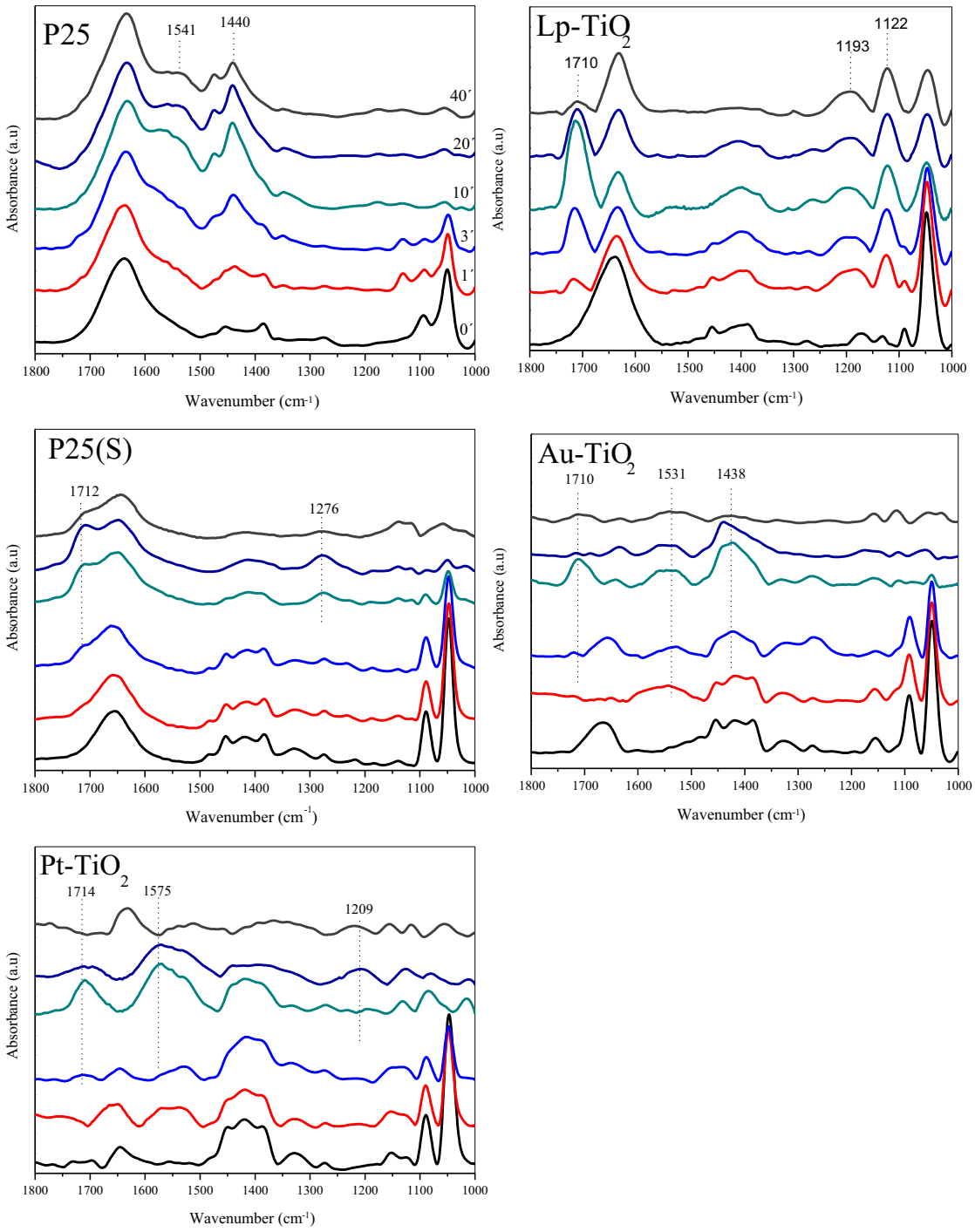

Fig. 9. FT-IR spectra for ethanol photo-oxidation over all analyzed photocatalysts.

surface (Scheme 4). In fact, a similar behavior was observed in the sulfated P25 sample, corroborating this hypothesis.

FT-IR studies of the NH_3 adsorption have revealed that the acid Lewis centers on lp-TiO_2 catalyst have a higher acid character than those observed on P25. It is possible that the sulfation treatment of P25 increases the acidity of the Lewis centers, suggesting that sulfate ions are close to these centers.

In metallized catalysts the acid strength of Lewis centers is also higher than in P25, but slightly lower than the one observed in lp-TiO_2. By FT-IR, a shifting of the bands assigned to surface sulfates was also observed on these samples. This shifting indicates clearly that sulfate interaction can be modified by addition of noble metals. Thus, metallized catalysts present a mechanism of ethanol photo-oxidation intermediate between those observed in the lp-TiO_2 and P25 samples.

As it has been indicated previously, in the metallized catalysts an ethanol–catalyst interaction by alcoholate formation cannot be ruled out, since the corresponding IR bands could be overlapping by the adjacent bands. Moreover, it has been reported that metal noble particles can act as breaking centers [40], providing an ethanol photo-oxidation mechanism similar to that observed in the P25.

The obtained results provided some useful information about mechanistic aspects of the ethanol photo-oxidation process over the different samples explaining the differences in selectivities. On

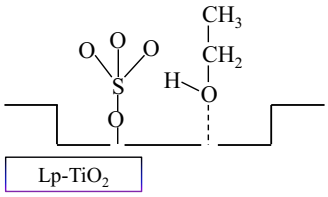

Scheme 4. Ethanol–Lp-TiO_2 interaction by hydrogen bonding.

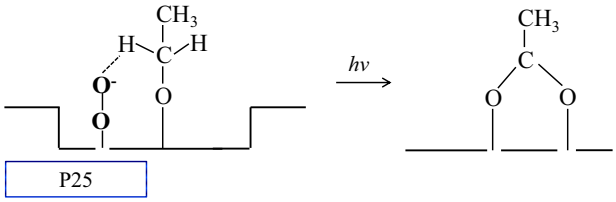

Scheme 5. Ethanol photo-oxidation mechanism over P25.

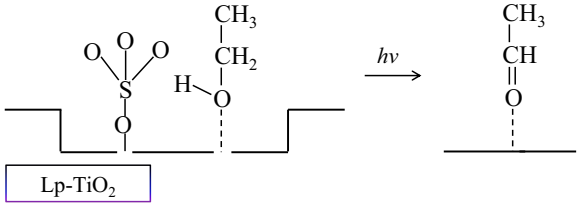

Scheme 6. Ethanol photo-oxidation mechanism over Lp-TiO_2.

P25, the ethanol photo-oxidation path is likely to occur through ethoxy species to yield acetate. The closeness of adsorbed oxygen can facilitate this mechanism (Scheme 5). By contrast in lp-TiO_2 a different surface distribution was observed, leading only to the aldehyde production (Scheme 6).

5. Conclusions

A FT-IR study of the hydroxylation state, ethanol adsorption and ethanol photocatalytic oxidation pathways over different photocatalysts was performed. For this study a pre-sulfated TiO_2 (lp-TiO_2), with and without noble metal deposition (Au and Pt) and TiO_2 P25 photocatalysts were evaluated.

FT-IR analyzes led us to propose different schemes about the ethanol–catalyst interaction, which allow explaining the ethanol photo-oxidation process observed on each studied photocatalyst.

It was found that sulfate ions adsorbed on the catalysts surface are closely related with the catalytic behavior observed during the ethanol photo-oxidation reaction. Thus, the ethanol–photocatalyst interaction and the photo-oxidation mechanism over the materials with and without sulfate pre-treatment were very different.

Thus, ethanol molecules interact with sulfated catalysts (lp-TiO_2 and sulfated P25) mainly through hydrogen bonding. Over these catalysts the ethanol is photocatalytically degraded to acetaldehyde.

On the other hand, ethanol interaction with pure P25 is given by alcoholate formation. Over this catalyst the ethanol photo-oxidation is faster than over the other analyzed photocatalysts; in this case the alcohol was transformed directly into acetates.

The deposition of noble metals on the TiO_2 surface also affected strongly the reaction pathway for ethanol photocatalytic oxidation, being strongly dependent on the kind of metal deposited. In metallized samples, the acid strength of Lewis centers lies between those observed in P25 and lp-TiO_2 giving rise to a combined mechanism in which acetaldehyde and acetates are formed as photo-oxidation products.

Au addition leads to a decrease of acetaldehyde selectivity, increasing the acetates production. Meanwhile Pt addition favors the formation of intermediates species, with lower amount of acetaldehyde and acetates production.

Acknowledgements

This research was financed by the Spanish MinisterioCiencia e Innovación (Project Ref. CTQ2011-26617-C03-02). J.J. Murcia would like to thank CSIC for the concession of a JAE grant and for financing the short stay no. 2012ESTCSIC – 7731. CITIUS (University of Seville) is acknowledged for XPS and XRF measurements.

References

[1] H. Idriss, E.G. Seebauer, Journal of Molecular Catalysis A: Chemical 152 (2000) 201–212.
[2] J.J. Murcia, M.C. Hidalgo, J.A. Navío, V. Vaiano, P. Ciambelli, D. Sannino, Catalysis Today 196 (2012) 101–109.
[3] P. Ciambelli, D. Sannino, V. Palma, V. Vaiano, R.S. Mazzei, Photochemical & Photobiological Sciences 8 (2009) 699–704.
[4] C. Della Pina, E. Falletta, L. Prati, M. Rossi, Chemical Society Reviews 37 (2008) 2077–2095.
[5] P. Pichat, Applied Catalysis B 99 (2010) 428–434.
[6] M.A. Henderson, Surface Science Reports 66 (2011) 185–297.
[7] A. Fujishima, X. Zhang, D.A. Tryk, Surface Science Reports 63 (2008) 515–582.
[8] G. Colón, M.C. Hidalgo, J.A. Navío, A. Kubacka, M. Fernández-García, Applied Catalysis B 90 (2009) 633–641.
[9] G. Colón, M.C. Hidalgo, G. Munuera, I. Ferino, M.G. Cutrufello, J.A. Navío, Applied Catalysis B 63 (2006) 45–59.
[10] M.C. Hidalgo, M. Maicu, J.A. Navío, G. Colón, Journal of Physical Chemistry C 113 (2009) 12840–12847.
[11] D. Kozlov, D. Bavykin, E. Savinov, Catalysis Letters 86 (2003) 169–172.
[12] D.S. Muggli, L. Ding, Applied Catalysis B 32 (2001) 181–194.
[13] J.C. Yu, J. Yu, J. Zhao, Applied Catalysis B 36 (2002) 31–43.
[14] M.C. Hidalgo, M. Maicu, J.A. Navío, G. Colón, Catalysis Today 129 (2007) 43–49.
[15] V. Iliev, D. Tomova, R. Todorovska, D. Oliver, L. Petrov, D. Todorovsky, M.U. Bujnova, Applied Catalysis A 313 (2006) 115–121.
[16] F. Denny, J. Scott, K. Chiang, W.Y. Teoh, R. Amal, Journal of Molecular Catalysis A: Chemical 263 (2007) 93–102.
[17] M.C. Hidalgo, J.J. Murcia, J.A. Navío, G. Colón, Applied Catalysis A 397 (2011) 112–120.
[18] J.J. Murcia, J.A. Navío, M.C. Hidalgo, Applied Catalysis B 126 (2012) 76–85.
[19] U.R. Pillai, E.S. Demessie, Journal of Catalysis 211 (2002) 434–444.
[20] L. Samiolo, M. Valigi, D. Gazzoli, R. Amadelli, Electrochimica Acta 55 (2010) 7788–7795.
[21] Z. Yu, S.S.C. Chuang, Journal of Catalysis 246 (2007) 118–126.
[22] D.V. Kozlov, E.A. Paukshtis, E.N. Savinov, Applied Catalysis B 24 (2000) L7–L12.
[23] S.P. Tandom, J.P. Gupta, Physical Status Solidi B 38 (1970) 363–367.
[24] A. Baylet, C. Capdeillayre, L. Retailleau, J.L. Valverde, P. Vernoux, A. Giroir-Fendler, Applied Catalysis B 102 (2011) 180–189.
[25] P.A. Connor, K.D. Dobson, A.J. McQuillan, Langmuir 15 (1999) 2402–2408.
[26] D. Peak, R.G. Ford, D.L. Sparks, Journal of Colloid and Interface Science 218 (1999) 289–299.
[27] S.J. Hug, Journal of Colloid and Interface Science 188 (1997) 415–422.
[28] T. Yamaguchi, Applied Catalysis 61 (1990) 1–25.
[29] S. Kataoka, E. Lee, M.I. Tejedor-Tejedor, M.A. Anderson, Applied Catalysis B 61 (2005) 159–163.
[30] B. Bonelli, M. Cozzolino, R. Tesser, M. Di Serio, M. Piumetti, E. Garrone, E. Santacesaria, Journal of Catalysis 246 (2007) 293–300.
[31] M. Primet, P. Pichat, M.V. Mathieu, Journal of Physical Chemistry 75 (1971) 1221–1226.
[32] L. Qingya, L. Zhenyu, L. Chengyue, Chinese Journal of Catalysis 27 (2006) 636–646.
[33] W.S. Kijlstra, D.S. Brands, H.I. Smit, E.K. Poels, A. Bliek, Journal of Catalysis 171 (1997) 219–230.
[34] G. Halasi, I. Ugrai, F. Solymosi, Journal of Catalysis 281 (2011) 309–317.
[35] J. Araña, J.M. Doña-Rodríguez, O. González-Díaz, E. Tello Rendón, J.A. Herrera Melián, G. Colón, J.A. Navío, J. Pérez Peña, Journal of Molecular Catalysis A: Chemical 215 (2004) 153–160.
[36] C.J. Pouchert, The Aldrich Library of Infrared Spectra, Aldrich Chemical Company, USA, 1981.
[37] S.M. Rao, A. Sridharan, Clays and Clay Minerals 32 (5) (1984) 414–418.
[38] H. Teterycz, R. Klimkiewicz, M. Laniecki, Applied Catalysis A 249 (2003) 313–326.
[39] M.D. Rhodes, A.T. Bell, Journal of Catalysis 233 (2005) 198–209.
[40] D. Uner, N.A.T.İ. Özen, M. Üner, Applied Catalysis A 251 (2003) 225–234.